Photocatalysis of Cyclooctane Dehydrogenation by the A-Frame Dinuclear Rhodium Complex $[Rh_2(\mu\text{-}S)(CO)_2(dppm)_2]$ [dppm = bis(diphenylphosphino)methane]†

Hiroaki Itagaki, Hisahiro Einaga and Yasukazu Saito*

Department of Industrial Chemistry, Faculty of Engineering, University of Tokyo, 7-3-1 Hongo, Bunkyo-ku, Tokyo 113, Japan

Visible-light irradiation at the longest-wavelength absorption band (λ_{max} = 475 nm) of the A-frame dinuclear complex $[Rh_2(\mu\text{-}S)(CO)_2(dppm)_2]$ [dppm = bis(diphenylphosphino)methane] caused catalytic dehydrogenation of cyclooctane [initial turnover frequency = 32.8 h^{-1}, total turnover number = 27.3 (per complex)]. The absorption band effective for photocatalysis was assigned to a metal-to-ligand charge transfer (m.l.c.t.) by extended Hückel molecular orbital (EHMO) calculations. The m.l.c.t. transition energy of $[Rh_2(\mu\text{-}S)(CO)_2(dppm)_2]$ was lower than that of the photocatalytically active mononuclear complex $[RhCl(CO)(PPh_3)_2]$ (λ_{max} = 364 nm), the origin of which was investigated in detail in terms of the Rh–Rh and Rh–S interactions.

The functionalization of saturated hydrocarbons under mild conditions is one of the most challenging targets in catalytic chemistry. Significant advances in the C–H bond activation of saturated hydrocarbons have been made with transition-metal complexes.[1] Recently, thermocatalytic dehydrogenation of cyclooctane in the absence of any hydrogen acceptors was achieved under boiling and refluxing conditions with the Wilkinson complexes $[RhCl(PR_3)_3]$ [R_3 = Ph_3, $MePh_2$ or $(C_6H_4Me\text{-}p)_3$].[2]

Photoirradiation of the Vaska-type rhodium complexes $[RhCl(CO)(PR_3)_2]$ gave extremely high dehydrogenation activities for alkanes [equation (1)].[3] Flash photolysis studies

$$C_nH_{2n+2} \longrightarrow C_nH_{2n} + H_2 \qquad (1)$$

revealed that photodissociation of CO from $[RhCl(CO)(PR_3)_2]$ (R = Ph, C_6H_4Me-*p* or Me) could generate a three-coordinated intermediate $[RhCl(PR_3)_2]$,[4] followed by the C–H bond splitting of the solvent cyclohexane, yielding $[RhCl(H)(C_6H_{11})(PR_3)_2]$ (R = Me).[4c,d] Photogenerated $[RhCl(PR_3)_2]$ is the key active species for alkane dehydrogenation.[3] We confirmed this from the wavelength dependence of photocatalytic activity for cyclohexane with $[RhCl(CS)(PPh_3)_2]$. The absorption band of $[RhCl(CS)(PPh_3)_2]$ (λ_{max} = 339 nm) effective for CS photodissociation leads to its dehydrogenation activity, whereas longer-wavelength photoirradiation (> 420 nm) was ineffective toward ligand dissociation so preventing catalytic reaction.[5] A quantumchemical interpretation was given in terms of molecular-orbital interactions.

In order to extend the effective wavelength for photocatalytic alkane dehydrogenation, we investigated the A-frame dinuclear rhodium complex $[Rh_2(\mu\text{-}S)(CO)_2(dppm)_2]$ [dppm = bis(diphenylphosphino)methane] on the grounds of its hydrogenation capability towards ethylene.[6] The wavelengths of the metal-to-ligand charge-transfer absorption bands of this dinuclear complex and those of related mononuclear complexes were estimated by extended Hückel molecular orbital (EHMO) calculations, taking into account metal–metal and metal–ligand interactions.

† *Non-SI unit employed:* eV ≈ 1.60 × 10^{-19} J.

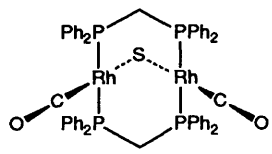

Experimental

All manipulations were carried out under an argon atmosphere. The complex $[Rh_2(\mu\text{-}S)(CO)_2(dppm)_2]$ was prepared by the published method[6] and the isolated complex recrystallized from CH_2Cl_2–MeOH. In order to remove any unsaturated hydrocarbons, reagent-grade cyclooctane was treated with a mixture of concentrated sulfuric and nitric acids, followed by drying over calcium chloride and distillation from sodium under a nitrogen atmosphere.

Photocatalyic dehydrogenation of neat cyclooctane was carried out under boiling and refluxing conditions (151 °C) in a cylindrical quartz cell (diameter 45 mm, cell length 80 mm), which was irradiated by an external-type xenon lamp (2 kW, Ushio) utilizing cut-off filters. Commercial glass cut-off filters, L-42, L-48 and L-60 (Kenko), were used; the L-42 filter was specified to cut off wavelengths < 420 nm (50% transmittance at 420 nm). The amount of gas evolved was measured with a gas burette (20 cm^3). The gas-phase products were analysed by gas chromatography using an active carbon column. The UV/VIS spectra of the reaction solution were recorded on a UV-365 (Shimadzu) spectrometer.

Calculations.—The extended Hückel method was adopted as a tool for interpreting the difference in λ_{max} values for mono- and di-nuclear rhodium complexes. Molecular geometries were calculated for $[Rh_2(\mu\text{-}S)(CO)_2(dppm)_2]$[6] and $[RhCl(CO)(PPh_3)_2]$[7] assuming C_{2v} symmetry and for $[\{RhCl(CO)(dppm)\}_2]$[8] assuming C_{2h} symmetry, respectively, with the bond lengths and angles taken from the crystal structures. Molecular orbital parameters such as valence state ionization potentials (v.s.i.p.) and Slater exponents for C(2s, 2p), O(2s, 2p),[9a] S(3s, 3p), Cl(3s, 3p) and Rh[5s, 5p, 4d(double ζ)][9b] were taken from the published values. As for the phosphine ligands,

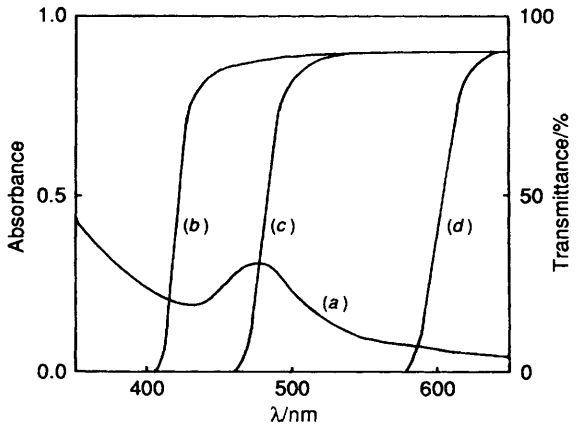

Fig. 1 UV/VIS spectrum of $[Rh_2(\mu\text{-}S)(CO)_2(dppm)_2]$ (*a*) with reference to transmission characteristics of the cut-off filters L-42 (*b*), L-48 (*c*) and L-60 (*d*); catalyst concentration 2.5 μmol per 100 cm^3 cyclooctane, cell length = 10 mm

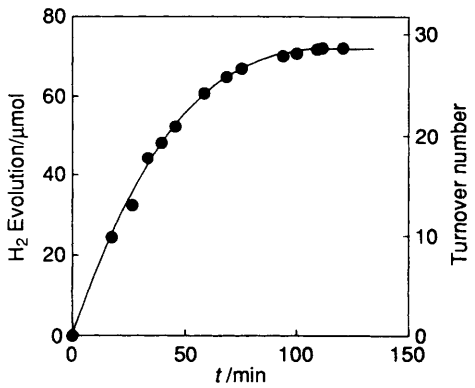

Fig. 2 Time-course plot for photocatalytic dehydrogenation of cyclooctane with $[Rh_2(\mu\text{-}S)(CO)_2(dppm)_2]$; catalyst concentration 2.5 μmol per 100 cm^3 cyclooctane, reaction temperature 151 °C (reflux), Xe lamp (2 kW) light source, L-42 cut-off filter

dppm and PPh_3 were replaced by two and one PH_3, respectively. In order to relate the properties of phosphine substituents to MO parameters more closely, both the v.s.i.p. and the Slater exponent of H in PH_3 were chosen so as to fit best the observed Rh–P NMR spin–spin coupling constants[10] within the framework of the Pople–Santry approximation.[11]

Results and Discussion

Photocatalytic Activity.—Fig. 1 shows the electronic absorption spectrum of $[Rh_2(\mu\text{-}S)(CO)_2(dppm)_2]$ together with the transmitting characteristics of the cut-off filters used for photoreactions. The longest-wavelength absorption maximum appeared in the visible region at 475 nm, longer than λ_{max} (364 nm)[12a] for $[RhCl(CO)(PPh_3)_2]$. This complex photodehydrogenated cyclooctane through the L-42 filter, giving a total turnover number of 27.3 (per complex, 2 h) (Fig. 2). Although stable in cyclooctane solution even under refluxing conditions (151 °C), the catalyst complex decomposed gradually upon photoirradiation, leading to a decrease of the catalytic activity with time. As shown in Table 1, a rather small initial rate and almost the same total turnover number were obtained under photoirradiation with the L-48 filter, whereas no H_2 was detected with the L-60 filter.

These results reveal that visible-light irradiation at the longest-wavelength band of $[Rh_2(\mu\text{-}S)(CO)_2(dppm)_2]$ is effective for catalytic dehydrogenation of cyclooctane. Similarly to the reaction mechanism of $[RhCl(CO)(PR_3)_2]$ (R = Ph, C_6H_4Me-*p* or Me), photoirradiation at the lowest-energy band causes CO dissociation, generating a reaction intermediate. Since the long-wavelength region (>420 nm) is ineffective for photocatalysis of mononuclear species, $[Rh_2(\mu\text{-}S)(CO)_2(dppm)_2]$ appears to retain its dinuclear structure during the reaction cycle.

Table 1 Wavelength dependence of photocatalytic dehydrogenation of cyclooctane with $[Rh_2(\mu\text{-}S)(CO)_2(dppm)_2]$*

Cut-off filter	Initial turnover frequency/h^{-1}	Total turnover number
L-42	32.8	27.3
L-48	24.9	26.9
L-60	0	0

* Catalyst concentration 2.5 μmol per 100 cm^3 cyclooctane; reaction temperature 151 °C (reflux), 2 h; light source Xe lamp (2 kW).

Quantumchemical Interpretation for the Longest-wavelength Absorption Band of $[Rh_2(\mu\text{-}S)(CO)_2(dppm)_2]$.—Quantumchemical calculations were carried out to elucidate the reason why $[Rh_2(\mu\text{-}S)(CO)_2(dppm)_2]$ shows a larger λ_{max} value than $[RhCl(CO)(PPh_3)_2]$. The effects of the apical S ligand, possible metal–metal interaction due to the rather short Rh–Rh distance (3.154 Å) and the Rh–S–Rh angle (83.5°) derived inherently from the A-frame structure[6] were compared with $[RhCl(CO)(PPh_3)_2]$ and a dinuclear H-frame complex $[\{RhCl(CO)(dppm)\}_2]$. An explanation of the CO photodissociation behaviour was also attempted to correlate with extended-Hückel molecular orbital properties.

Assignment of the electronic spectrum of $[Rh_2(\mu\text{-}S)(CO)_2(dppm)_2]$. According to electronic[12a] and magnetic circular dichroism (MCD) spectral[12b] studies, the absorption band of $[RhCl(CO)(PPh_3)_2]$ (364 nm) was assigned as the allowed m.l.c.t. transition from an occupied rhodium d orbital to a vacant CO π-acceptor orbital. EHMO calculations assigned this band as the electronic transition from the highest occupied molecular orbital (HOMO) to an unoccupied MO, both being constituted mainly of $Rh(d_\pi)$ and $CO(\pi^*)$ orbitals {*cf.* $6b_1$ and $8b_1$ orbitals of $[RhCl(CO)(PPh_3)_2]$ in Fig. 4}. Antibonding interactions between the Rh and C atoms in unoccupied MOs would induce CO dissociation, generating a three-co-ordinated reaction intermediate.[5]

The longest-wavelength absorption band (475 nm) of $[Rh_2(\mu\text{-}S)(CO)_2(dppm)_2]$ is assignable to an m.l.c.t. transition on the basis of its similar ε_{max} value (6600 $dm^3\ mol^{-1}\ cm^{-1}$) to that (3780 $dm^3\ mol^{-1}\ cm^{-1}$)[12a] of $[RhCl(CO)(PPh_3)_2]$, suggesting an electronic transition from an occupied to an unoccupied MO of mainly $Rh(d_\pi)$ and $CO(\pi^*)$ character.

Candidate MOs (and their energy levels) for the m.l.c.t. transition of $[Rh_2(\mu\text{-}S)(CO)_2(dppm)_2]$ are shown in Fig. 3. Since the phosphine orbitals were either negligibly weakly or non-bonding with $Rh(d_\pi)$ orbitals in all these MOs, the orbitals shown here were limited to Rh, S, C and O. The HOMO is constructed from $Rh(d_\pi)$, $CO(\pi^*)$ and $S(p_\pi)$ orbitals and shows bonding Rh–C and antibonding Rh–S interactions, respectively. It is to be noted that the energy level of the occupied orbital $10b_2$ consisting of mutually antibonding $Rh(d_\sigma)$ orbitals is rather lower in energy (−12.64 eV) (see below). All of the candidate unoccupied MOs, *i.e.* $15a_1$, $13b_2$, $14a_2$ and $11b_1$, were made up mainly of $Rh(d_\pi)$ and $CO(\pi^*)$ orbitals with antibonding Rh–C interactions. The absorption band at 475 nm can be assigned to the HOMO ⟶ $15a_1$ transition, since this m.l.c.t. transition is allowed on symmetry grounds and is of the lowest energy among the viable choices.† The $15a_1$ orbital

† Even if the absorption band arises from the HOMO ⟶ $14a_2$ and/or HOMO ⟶ $11b_1$ transition(s) together with the HOMO ⟶ $15a_1$ transition, all would contribute to the CO photodissociation due to the Rh–C antibonding interactions in these orbitals.

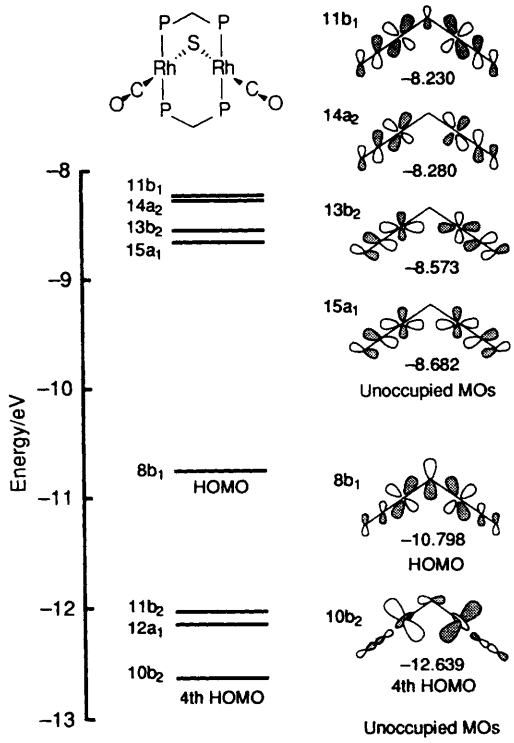

Fig. 3 Candidate MOs for electronic transition in $[Rh_2(\mu\text{-}S)(CO)_2(dppm)_2]$

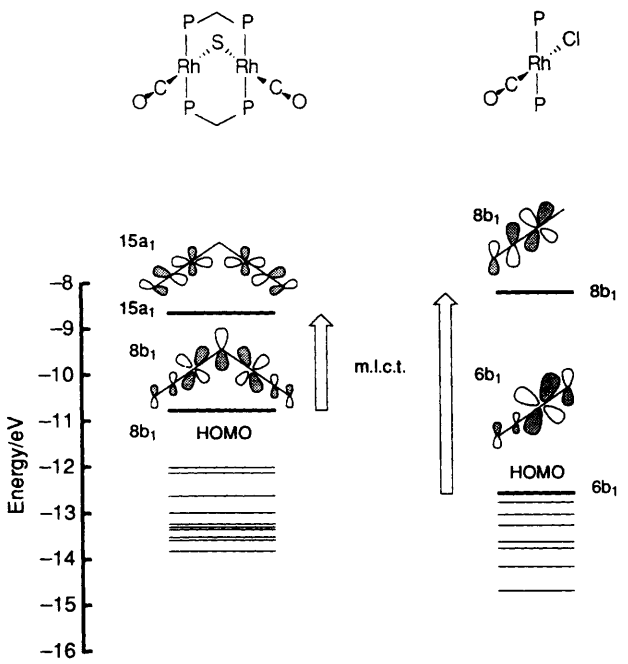

Fig. 4 Energy levels and molecular orbitals assignable to electronic transitions in $[Rh_2(\mu\text{-}S)(CO)_2(dppm)_2]$ and $[RhCl(CO)(PPh_3)_2]$

exhibited large antibonding interactions between the $Rh(d_\pi)$ and $C(p_\pi)$ orbitals, whereas both Rh–S and Rh–P bonds were non-bonding. Thus, the m.l.c.t. transition to $15a_1$ will cause cleavage of the Rh–CO bond, while the Rh–S and Rh–P bonds remain intact.[5]

Comparison of m.l.c.t. absorption bands between $[Rh_2(\mu\text{-}S)(CO)_2(dppm)_2]$ *and* $[RhCl(CO)(PPh_3)_2]$. Fig. 4 shows the energy levels of molecular orbitals relevant to m.l.c.t. transitions in $[Rh_2(\mu\text{-}S)(CO)_2(dppm)_2]$ and $[RhCl(CO)(PPh_3)_2]$. The

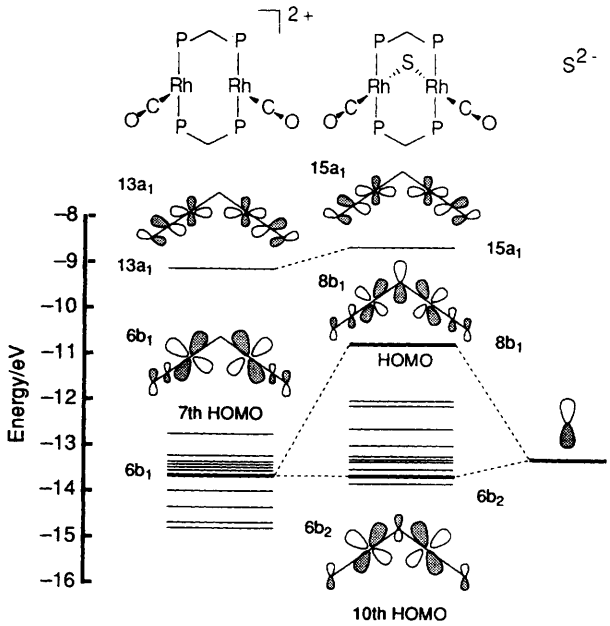

Fig. 5 Interaction diagram of $6b_2$, $15a_1$ and $8b_1$ orbitals important for electronic transitions in $[Rh_2(\mu\text{-}S)(CO)_2(dppm)_2]$

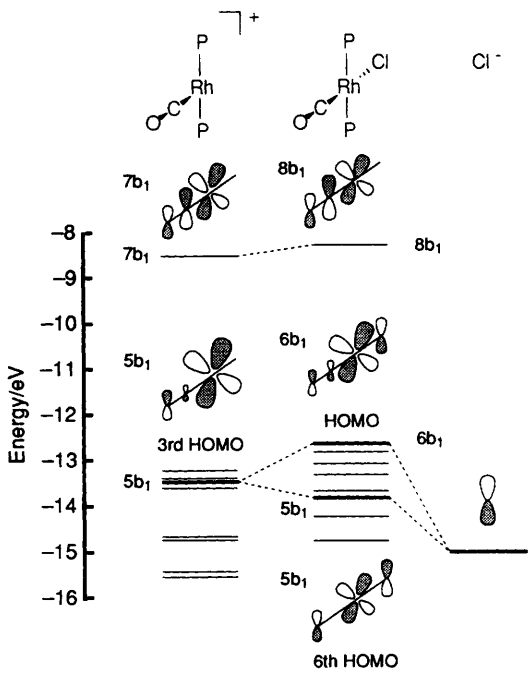

Fig. 6 Interaction diagram of $5b_1$, $8b_1$ and $6b_1$ orbitals important for electronic transitions in $[RhCl(CO)(PPh_3)_2]$

transition energy calculated for $[Rh_2(\mu\text{-}S)(CO)_2(dppm)_2]$ (2.12 eV) was apparently smaller than that (4.38 eV) for $[RhCl(CO)(PPh_3)_2]$, in accord with the larger λ_{max} value for the dinuclear complex.

The EHMO interaction diagrams for $[Rh_2(\mu\text{-}S)(CO)_2(dppm)_2]$ built up from the fragments $\{Rh_2(CO)_2(dppm)_2\}^{2+}$ and S^{2-}, and for $[RhCl(CO)(PPh_3)_2]$ from $\{Rh(CO)(PPh_3)_2\}^{+}$ and Cl^- are shown in Fig. 5 and Fig. 6, respectively. Upon co-ordination of S^{2-} to $\{Rh_2(CO)_2(dppm)_2\}^{2+}$, the orbital energies of the unoccupied MOs changed little (0.48 eV), as ascertained with respect to $13a_1$ (Fig. 5). Similarly, little influence (0.28 eV) was exerted upon co-ordination of Cl^- to $\{Rh(CO)(PPh_3)_2\}^{+}$, as shown for $7b_1$ (Fig. 6). These small

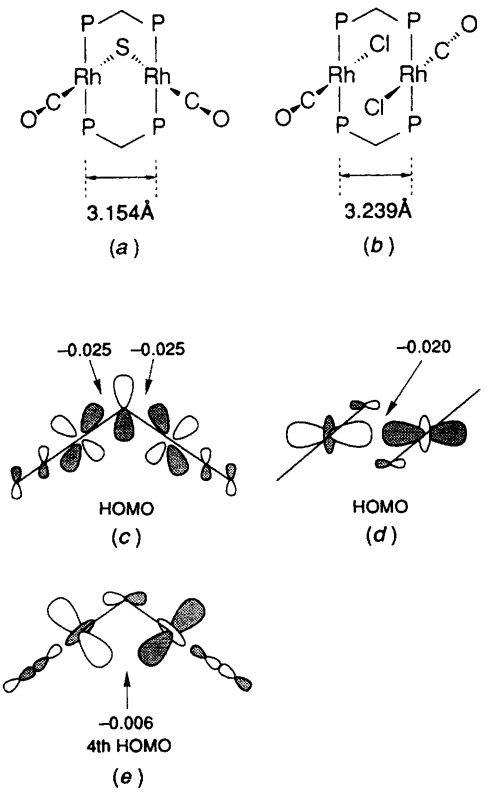

Fig. 7 Atomic orbital bond populations and Rh–Rh distances (in Å) for $[Rh_2(\mu\text{-}S)(CO)_2(dppm)_2]$ and $[\{RhCl(CO)(dppm)\}_2]$

energy changes indicated the absence of substantial contributions of the S and Cl orbitals in influencing photodissociative behaviour.

A sharp contrast can be pointed out for the HOMO orbitals of $[Rh_2(\mu\text{-}S)(CO)_2(dppm)_2]$ (Fig. 5) and $[RhCl(CO)(PPh_3)_2]$ (Fig. 6). Energy elevation from the fragment orbitals was large for the former (2.85 eV from the $6b_1$ orbital) but small for the latter (0.84 eV from the $5b_1$ orbital), which should be responsible for the smaller m.l.c.t. transition energy of the A-frame complex relative to $[RhCl(CO)(PPh_3)_2]$.

Consequently, we conclude that the large λ_{max} value, *i.e.* the small m.l.c.t. transition energy for $[Rh_2(\mu\text{-}S)(CO)_2(dppm)_2]$ originates from its high-energy lying HOMO.

Molecular-orbital interpretation of the HOMO energy level of $[Rh_2(\mu\text{-}S)(CO)_2(dppm)_2]$. The remarkable energy level promotion calculated for the HOMO orbital of the A-frame complex can be interpreted in terms of energy levels and orbital interactions of the fragment MOs by comparing them with those of $[RhCl(CO)(PPh_3)_2]$ and the H-frame $[\{RhCl(CO)(dppm)\}_2]$ complexes.

The $Cl(p_\pi)$ orbital energy of $[RhCl(CO)(PPh_3)_2]$ is calculated to be lower than its filled fragment $\{Rh(CO)(PPh_3)_2\}^+$ $5b_1$ orbital by 1.50 eV. On the contrary, the energy of $S(p_\pi)$ (−13.30 eV) was almost equal to that of the fragment $\{Rh_2(CO)_2(dppm)_2\}^{2+}$ $6b_1$ MO level (−13.63 eV) in the A-frame complex, which is very important because of its contribution to high energy-level promotion of the HOMO.

In order to obtain more precise insight into the $Rh(d_\pi)$–$S(p_\pi)$ and $Rh(d_\sigma)$–$Rh(d_\sigma)$ orbital interactions, atomic orbital bond populations (a.o.b.p.), $C_{rj}C_{sj}S_{rs}$ (C = molecular-orbital coefficient, S = overlap integral), were calculated for both A- and H-frame complexes (Fig. 7), since bonding interaction between atoms r and s in a molecular orbital j (j = HOMO or 4th HOMO in this case) is well represented by this parameter.

In the H-frame complex,[13] the high orbital energy of its HOMO is caused by an antibonding $Rh(d_\sigma)$–$Rh(d_\sigma)$ interaction (a.b.o.p. = −0.020) [Fig. 7(*d*)] due to its short Rh–Rh distance (3.239 Å) [Fig. 7(*b*)]. The Rh–Rh distance of the A-frame complex (3.154 Å) [Fig. 7(*a*)] is shorter than that of the H-frame (3.239 Å) yet the a.o.b.p. value of the antibonding $Rh(d_\sigma)$–$Rh(d_\sigma)$ interaction [Fig. 7(*e*)] for the corresponding MO of the A-frame complex was rather small (−0.006) owing to the inherent Rh–S–Rh angle (83.5°)[6] leading to a weaker interaction between the mutually antibonding $Rh(d_\sigma)$ orbitals and the deep energy level of the $10b_2$ orbital (4th HOMO).

On the other hand, an intense and antibonding $Rh(d_\pi)$–$S(p_\pi)$ interaction is estimated for the A-frame complex. The rather large negative a.o.b.p. value of −0.025 [Fig. 7(*c*)] should be another quantumchemical reason leading to the remarkably high HOMO level.

The long wavelength m.l.c.t. absorption for $[Rh_2(\mu\text{-}S)(CO)_2(dppm)_2]$ is thus well correlated by EHMO calculations concerning transition energies and orbital interactions. A molecular design of photocatalysts effective for alkane dehydrogenation under visible-light irradiation will be useful to the chemical conversion of solar energy.

Conclusion

The effectiveness of visible light for catalytic dehydrogenation of cyclooctane was established for the A-frame dinuclear complex $[Rh_2(\mu\text{-}S)(CO)_2(dppm)_2]$ (λ_{max} = 475 nm). For this complex the longest-wavelength absorption band was assigned to an m.l.c.t. transition from the HOMO ($8b_1$) to an unoccupied orbital ($15a_1$).

The difference in transition energies between $[Rh_2(\mu\text{-}S)(CO)_2(dppm)_2]$ and $[RhCl(CO)(PPh_3)_2]$ was ascribed to the difference in energy levels of the HOMO in each complex. The high energy level of the HOMO in $[Rh_2(\mu\text{-}S)(CO)_2(dppm)_2]$ is caused by two factors; (*i*) the energy levels of the $S(p_\pi)$ and the fragment $\{Rh_2(CO)_2(dppm)_2\}^{2+}$ $6b_1$ orbitals are almost equal and (*ii*) the $S(p_\pi)$ orbital has antibonding interactions with the two $Rh(d_\pi)$ orbitals.

In contrast to the H-frame $[\{RhCl(CO)(dppm)\}_2]$ complex, the inherent Rh–S–Rh angle (83.5°) of $[Rh_2(\mu\text{-}S)(CO)_2(dppm)_2]$ causes the antibonding $Rh(d_\sigma)$–$Rh(d_\sigma)$ interaction to be insignificant.

References

1 R. H. Crabtree, *Chem. Rev.*, 1985, **85**, 245; R. G. Bergman, P. F. Seidler and T. T. Wenzel, *J. Am. Chem. Soc.*, 1985, **107**, 4358; J. M. Buchanan, J. M. Stryker and R. G. Bergman, *J. Am. Chem. Soc.*, 1986, **108**, 1537; R. A. Periana and R. G. Bergman, *J. Am. Chem. Soc.*, 1986, **108**, 7332 and refs. therein.
2 T. Fujii and Y. Saito, *J. Chem. Soc., Chem. Commun.*, 1990, 757; T. Fujii, Y. Higashino and Y. Saito, *J. Chem. Soc., Dalton Trans.*, 1993, 517.
3 K. Nomura and Y. Saito, *J. Chem. Soc., Chem. Commun.*, 1988, 161; T. Sakakura, T. Sodeyama, Y. Tokunaga and M. Tanaka, *Chem. Lett.*, 1988, 263; J. A. Maguire, W. T. Boese and A. S. Goldman, *J. Am. Chem. Soc.*, 1989, **111**, 7088; K. Nomura and Y. Saito, *J. Mol. Catal.*, 1989, **54**, 57; T. Sakakura, T. Sodeyama and M. Tanaka, *New J. Chem.*, 1989, **13**, 737; J. A. Maguire, W. T. Boese, M. E. Goldman and A. S. Goldman, *Coord. Chem. Rev.*, 1990, **97**, 179; M. Tanaka and T. Sakakura, *Pure Appl. Chem.*, 1990, **6**, 1147.
4 (*a*) D. A. Wink and P. C. Ford, *J. Am. Chem. Soc.*, 1985, **107**, 1794; (*b*) D. A. Wink and P. C. Ford, *J. Am. Chem. Soc.*, 1987, **109**, 436; (*c*) C. T. Spillett and P. C. Ford, *J. Am. Chem. Soc.*, 1989, **111**, 1932; (*d*) P. C. Ford, T. L. Netzel, C. T. Spillett and D. B. Pourreau, *Pure Appl. Chem.*, 1990, **62**, 1091.
5 A. Iwamoto, H. Itagaki and Y. Saito, *J. Chem. Soc., Dalton Trans.*, 1991, 1093.
6 C. P. Kubiak and R. Eisenberg, *Inorg. Chem.*, 1980, **19**, 2726.
7 A. Ceriotti, G. Ciani and A. Sironi, *J. Organomet. Chem.*, 1983, **247**, 345.
8 M. Cowie and S. K. Dwight, *Inorg. Chem.*, 1980, **19**, 2500.
9 (*a*) R. H. Summerville and R. Hoffmann, *J. Am. Chem. Soc.*, 1976, **98**, 7240; (*b*) D. M. Hoffman and R. Hoffmann, *Inorg. Chem.*, 1981, **20**, 3543.

10 H. Itagaki, Y. Saito and S. Shinoda, *J. Mol. Catal.*, 1987, **41**, 209.
11 J. A. Pople and D. P. Santry, *Mol. Phys.*, 1964, **8**, 1.
12 (*a*) R. Brady, B. R. Flynn, G. L. Geoffroy, H. B. Gray, J. Peone, jun. and L. Vaska, *Inorg. Chem.*, 1976, **15**, 1485; (*b*) G. L. Geoffroy, H. Isci, J. Litrenti and W. R. Mason, *Inorg. Chem.*, 1977, **16**, 1950.
13 A. L. Balch and B. Tulyathan, *Inorg. Chem.*, 1977, **16**, 2840.

Received 17*th December* 1992; *Paper* 2/06688B